2025 IEEE/SICE International Symposium on System Integration (SII)
January 21-24, 2025, Munich, Germany

Roddy: Rod Elasticity Incorporated into a Robot Manipulator for Rigid Tool Use around Rigid Environment

Terumi Tokuyama[1] and Hiromi Mochiyama[1]

***Abstract*— In order to enhance the capability of soft robot manipulator, we propose Roddy, a new type of soft robot system for manipulating a "rigid" tool softly. In Roddy, an elastic rod with a 6-axis force sensor is inserted in series between a rigid tool and a rigid robot manipulator. By utilizing the real-time shape estimation technology, Roddy can recognize the rigid tool position/orientation relative to a rigid environment with high accuracy and precision. Due to high compliance of Roddy, we can achieve accurate calibration of the manipulator tool relative to the environmental flat plane. Moreover, we can also achieve to map the location of obstacles on a plane by exploratory collisions. Based on this obstacle mapping algorithm, we demonstrate that Roddy can safely achieve quick scooping tasks where the rigid tool of the robot manipulator is continuously contact with the environmental rigid plane.**

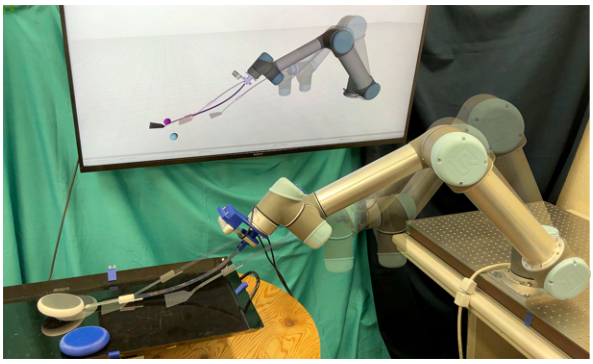

Fig. 1. Roddy: A robotic manipulator with rod elasticity with real-time shape estimation by force sensing.

I. INTRODUCTION

Robots have evolved rapidly in recent years, but there are still tasks that humans can easily perform but robots cannot. Normally, humans can accomplish dexterous tasks by utilizing rigid tools to take full advantage of rigid surfaces in the environment, despite collisions between rigid objects. Such tasks include quickly scooping the food on the hard griddle with a hard utensil, e.g., a spatula. The purpose of our research is to extend the capabilities of robots by enabling them to perform tasks that humans can do but robots cannot currently accomplish. In this paper, we will focus on the quick scooping tasks mentioned above. Achieving this goal is expected to improve the capabilities of cooking robots.

A quick scooping task is characterized by the following nonconventional contact conditions:

1) Hard-hard contact: A hard tool at the tip of the robot comes into contact with a hard environment.
2) Edge-plane contact: The edge of the tool may come into contact with a plane of the environment.
3) Continuously-changing contact location: The contact location of the edge relative to the plane may change continuously.

A possible way to dealing with the fore-mentioned non-conventional hard contact conditions is to employ impedance control together with conventional rigid robot manipulators [1]. However, such control solution requires implementation of real-time control with very short sampling time which costs much. Recent advances in imitation learning techniques have also made it possible to achieve hard contact tasks with the environment [2]-[4]. However, the cost of learning is high, and only tasks that could be operated by humans can be learned. In addition, the generality of this type of AI controllers is also limited, so only limited compliance characteristics can be expected. Therefore, it is desirable to embed intrinsic compliance into manipulators by series elasticity [5][6]. However, it is difficult to achieve multi-degree-of-freedom compliance while accurately determining the position and orientation of the rigid tool attached to the tip of the manipulator.

In this paper, we propose a new type of soft robot system for manipulating a "rigid" tool softly, named Roddy. In Roddy, an elastic rod with a 6-axis force sensor is inserted in series between a rigid tool and a rigid robot manipulator. By utilizing the real-time shape estimation technology [8][9], Roddy can recognize the rigid tool position/orientation relative to a rigid environment with high accuracy and precision. Therefore, quick scooping tasks can be realized by Roddy.

The contributions of this research are as follows:

- Multi-Degree-of-Freedom Collision Mitigation by Implementation of a Robotic System Incorporating Rod Elasticity into a Manipulator in Series
- Development of obstacle mapping algorithm with exploratory collision based on real-time shape estimation technique including an end effector
- Demonstration of the capability of soft robotic manipulators by achieving quick scooping tasks

II. PROPOSED SYSTEM

A. Concept

The proposed robot system, Roddy, is a kind of soft robots. This consists of

This work was supported by the University of Tsukuba and the Japan Society for the Promotion of Science (KAKENHI) under Grant JP23H01372.

[1]Terumi Tokuyama and Hiromi Mochiyama are with FlexibleRobotics Laboratory, University of Tsukuba, 1-1-1 Tennoudai, Tsukuba, Ibaraki 305-8573, Japan (email: s2320770@u.tsukuba.ac.jp; motiyama@iit.tsukuba.ac.jp).

1) an elastic rod,
2) a 6-axis force/torque sensor,
3) a rigid tool,
4) a rigid motion base,
5) a controller including the real-time rod shape estimation algorithm, and
6) a rigid environment.

One end of the elastic rod is fixed to the force/torque sensor while the other end is connected with the rigid tool. The motion base is used for rigidly moving the position and orientation of the force/torque sensor. The real-time rod shape estimation algorithm allows real-time calculation of the shape of an elastic rod from 6-axis forces/torques measured by the force/torque sensor. For details, see [8][9]. As a result, the tip position and orientation of the elastic rod can be obtained.

If the rod is rigid, this robotic system is nothing more than a conventional robotic manipulator. However, the elastic rod used in this system is actually highly flexible. Therefore, this robotic manipulator is highly compliant in all directions due to the hyper many-degree-of-freedom nature of a highly flexible rod. Despite this high compliance characteristic, due to the real-time shape estimation algorithm by force sensing, the position and orientation of the rigid tool can be estimated with sufficient accuracy. This compatibility between high compliance and tip accuracy is the outstanding feature of this robot system. Based on this distinguished feature, Roddy is expected to enable non-conventional tasks using a rigid tool intentionally brought into contact with a rigid environment.

B. Prototype

Here we describes a prototype of Roddy that was constructed to validate the effectiveness of Roddy. This prototype consists of

1) a hardening steel strip with a size of 300x20x0.4[mm],
2) a strain-sensing type 6-axis force/torque sensor (FFS055F100M1R0U6S, Leptrino Co. Ltd.),
3) a stainless steel spatula for griddling
4) a serial-chain manipulator (UR5, Universal Robots Inc.)
5) a ROS PC with the real-time rod shape estimation algorithm with gravity consideration [9], and
6) a flat steel plate for griddling.

Figure 2 illustrates the prototype of Roddy where 1) a spatula as a rigid tool, 2) a thin hardening steel strip as an elastic rod, 3) a 6-axis force sensor, and 4) a UR5 as a motion base are connected in series. In the implementation for acquiring each coordinate of Roddy, the measured values from the 6-axis force sensor are sent to the computer via serial communication. The frame at the tip of the Rigid Motion Base is acquired and used as the base frame for calculations utilizing real-time rod shape estimation. The Rigid Motion Base's pose information is obtained using ROS, and the position and orientation of the elastic rod are estimated from the force/torque data. The estimated pose can be visualized with RViz and qualitatively compared with the actual pose of Roddy. The motion planning framework MoveIt is used to control the movement of the Rigid Motion Base. Each link and joint is described in XML format using URDF and Xacro files, and the estimated position and orientation of Roddy are updated according to the calculation results. Consequently, Roddy can estimate the position and posture of the rigid tool in real-time. Roddy can be regarded as a hyper multi-degree-of-freedom extension of a series elastic actuator.

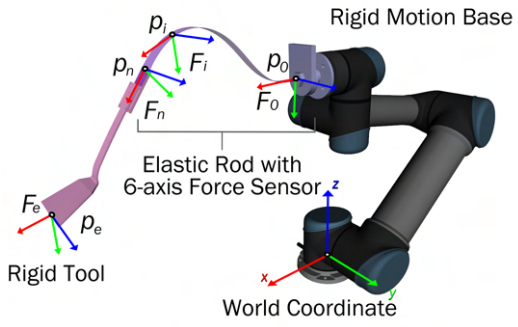

Fig. 2. Roddy prototype. An elastic rod with a 6-axis force sensor is incorporated between a rigid tool (spatula) and a rigid motion base (UR5). The real-time rod shape estimation algorithm allows accurate estimation of tool position and orientation. This enables hyper many-degree-of-freedom series elasticity.

C. Calibration based on Line-Plane Contact

High compliance of Roddy enables to move the rigid tool with maintaining contact with a rigid flat plane as an environment. Based on this property, we propose an almost automatic, accurate calibration method of the manipulator tool relative to the environmental flat plane.

Let $\boldsymbol{l} : [0\ 1] \times [0\ \infty) \rightarrow \Re^3$ be the trajectory of the line segment corresponding to the tip edge of the spatula. Explicitly, $\boldsymbol{l}(s,t) = (1-s)\boldsymbol{l}_0(t) + s\boldsymbol{l}_1(t)$ denotes the position vector of the point on the edge line segment at the line parameter $s \in [0\ 1]$ at time $t \in [0\ \infty)$ where $\boldsymbol{l}_0$ and $\boldsymbol{l}_1 \in \Re^3$ are the position vectors of the corner points of the spatula. Suppose the environmental rigid plane which is denoted by $\mathcal{P} \subset \Re^3$. Due to high compliance nature of Roddy, the tool tip of Roddy can be moved with maintaining contact with the flat plane. This line-plane contact situation can be expressed by

$$\boldsymbol{l}(s,t) \subset \mathcal{P} \tag{1}$$

with $s \in [0\ 1]$ and $t \in [0\ \infty)$.

The purpose of the calibration here is to obtain the expression of the estimated rigid plane $\hat{\mathcal{P}}$ relative to the manipulator's world coordinate. Thanks to the rod shape estimation algorithm, $\boldsymbol{l}(s,t)$ can be estimated in real time. Let $\hat{\boldsymbol{l}}(s,t) \in \Re^3$ be the estimated value of $\boldsymbol{l}(s,t)$. Suppose that we conduct the rod shape estimation at the time $t = t_0, t_1, \cdots, t_{N_t-1}$ where N_t is the number of estimation. We also select the points on the line segment whose line

parameters are $s = s_0, s_1, \cdots, s_{N_s-1}$ where N_s is the number of the selected points. Then,

$$\begin{aligned} &\hat{\boldsymbol{l}}(s_0, t_0),\ \hat{\boldsymbol{l}}(s_1, t_0),\ \cdots,\ \hat{\boldsymbol{l}}(s_{N_s}, t_0), \\ &\hat{\boldsymbol{l}}(s_0, t_1),\ \hat{\boldsymbol{l}}(s_1, t_1),\ \cdots,\ \hat{\boldsymbol{l}}(s_{N_s}, t_1), \\ &\vdots \\ &\hat{\boldsymbol{l}}(s_0, t_{N_t-1}),\ \hat{\boldsymbol{l}}(s_1, t_{N_t-1}),\ \cdots,\ \hat{\boldsymbol{l}}(s_{N_s}, t_{N_t-1}) \end{aligned} \quad (2)$$

forms the point cloud distributed around the flat plane $\mathcal{P}$. Therefore, from this point cloud, the estimated flat plane $\hat{\mathcal{P}}$ can be computed accurately by using some efficient algorithm to calculate a plane.

D. Mapping of Obstacles by Exploratory Collisions

Roddy's high compliance allows it to intentionally collide with obstacles in order to learn environmental information. Here, we propose an algorithm that maps the location of obstacles on a plane by exploratory collisions.

The rod shape estimation algorithm allows us to estimate the shape of an elastic rod even if any external forces and torques are applied to the rigid tool at the tip. On the other hand, it is difficult to accurately estimate the contact point of the external force and torque applied on the tool from the measured force and torque at the base of the elastic rod even a single contact case. Therefore, we will take a strategy of exploratory collisions.

Suppose the manipulator moves forward and makes a single contact with the edge of the rigid tool. In this case, a large impact force in the opposite direction of the forward motion is observed, which can be used to detect a collision. From noisy and impulsive force and torque measurements, it may be difficult to accurately estimate the collision location at the tool edge. However, from the measured force and torque data profile, $\boldsymbol{f}_s(t), \boldsymbol{m}_s(t) \in \Re^3$, it is quite possible to identify collisions in the center, on the right side, and on the left side of the tool edge.

Let $\gamma_{\Delta t} : \Re^{6\times\Delta t} \times [0\ \infty) \to \{'\text{Center}', '\text{Left}', '\text{Right}'\}$ be the function of the contact location on the tool from the measured force/torque profile $\boldsymbol{f}_s(t), \boldsymbol{m}_s(t)$ with the time window Δt around the collision time t^*. If the collision is judged to have occurred on the right side of the tool edge from the measured force/torque data profile, i.e., $\gamma_{\Delta t}$ ='Right', the manipulator slightly moves backward, steps right, and moves forward again. On the other hand, if $\gamma_{\Delta t}$ ='Left', it steps back and left, and moves forward again. By repeating these motions until $\gamma_{\Delta t}$ ='Center', it is highly expected that the collision is sufficiently around the center of the edge. Therefore, the estimated obstacle position $\hat{\boldsymbol{p}}_{\text{obs}}$ can be evaluated to be equal to the center point of the tool edge $\boldsymbol{p}_{\text{tool}} \in \hat{\mathcal{P}}$, that is, $\hat{\boldsymbol{p}}_{\text{obs}} = \boldsymbol{p}_{\text{tool}}$.

The proposed obstacle mapping algorithm is described in **Algorithm 1**.

Algorithm 1 Obstacle Mapping by Exploratory Collisions

```
p_tool ∈ P̂.
while No Collision do
  Move Forward.
  repeat
    if Collision Detected then
      Stop. t* = t.
      if γ_Δt = 'Right' then
        Step Back. Step Right. Move Forward.
      else if γ_Δt = 'Left' then
        Step Back. Step Left. Move Forward.
      else
        p̂_obs = p_tool.
      end if
    end if
  until γ_Δt = 'Center'
end while=0
```

III. EXPERIMENTS

This section describes three experiments to validate the effectiveness of Roddy in terms of calibration accuracy, obstacle mapping accuracy, and quick scoop feasibility.

A. Calibration Accuracy

The calibration method proposed in II-C is validated by showing the accuracy of the relative plane angle estimation.

1) Method:

- A flat steel plate as an environmental rigid plane is fixed to the ground via a rotational stage (Fig. 3-c) that can be manually angled. The relative plate angle is set to 0, ±3 and ±5 degree.
- The initial configuration of the motion base is set so that the height of the tool tip is sufficiently lower than the height of the flat plate when the flat plate is removed. The high compliance of the roddy ensures that the contact between the tool edge and the plate is maintained during the horizontal motion of the motion base tip, that is $\boldsymbol{l} \subset \mathcal{P}$.
- The motion base tip is moved forward 0.20 meters, backward by 0.20 meters, and left 0.03 meters, at a speed of 0.05 m/s. This process is repeated until the path covers the entire flat surface of the plate. The total process is defined as a trial. We conducts 5 trials for each relative plate angle.
- During each trial, the position and orientation of the tool is estimated by the shape estimation algorithm in real time, and the center position of the tool edge is recorded at about 10 Hz. Based on the collected data, the point cloud of the tool edge (2) is obtained, where the total number of the date $N_s \times N_t$ is from 1,070 to 1,080.
- In order to obtain the estimated plane $\hat{\mathcal{P}}$ from the point cloud, RANSAC[10] is used. The residual threshold used for data fitting is set to the median error of the point cloud.

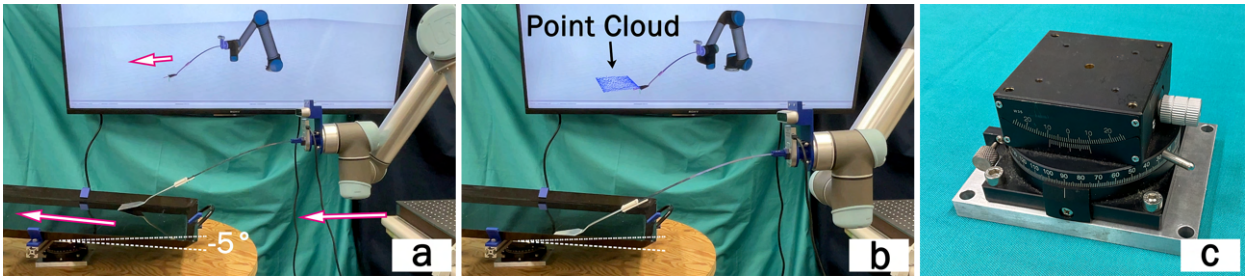

Fig. 3. Setup for the calibration accuracy experiment. (a) The rigid spatula attached to the end of the motion base via an elastic rod moves straight on the steel plate while maintaining contact between the tool edge and the steel plate due to the flexibility of the rod, during the linear motion of the motion base. In this case, the inclination angle of the steel plate is set to -5 degrees on the rotational stage. (b) A point cloud is formed by repeating the actions of moving forward, backward, and to the left while recording the center position of the blade tip of the spatula. It can be seen that the point cloud is displayed as a flat shape on the screen. (c) The rotational stage for setting the inclination angle of the steel plate.

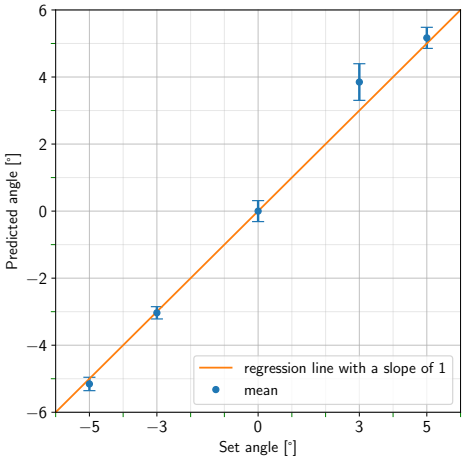

Fig. 4. Error bar graph in which the dots represent the mean of the data and the error bars represent the standard deviation. For comparison, a simple regression with a slope of 1 is added in orange.

2) Result: The angle set by the rotational stage was compared with the angle estimated from the plane equation obtained in the experiment, as shown in Fig. 4. The vertical axis represents the estimated angle while the horizontal axis represents the set angle. Because five trials were conducted for each set angle, 25 sets of the point clouds were obtained. The mean and standard deviation of the five trials for each angle were plotted (circles for mean values, error bars for standard deviations). The estimated angle was plotted relative to the angle when the set angle was 0 degrees. A plot on a line with a slope of 1 and an intercept of 0 means perfect estimation. The graph shows that even with high manipulator flexibility and nearly automatic calibration, the relative plate inclination can be estimated with high accuracy.

The angle between the spatula and the rigid plate is considered to be an important factor in achieving the scooping task. In Fig. 4, when the angle of the plate is set to 3 degrees, it can be seen that the error in the estimated plane angle increases. This is thought to be due to the fact that the friction between the spatula and the rigid plate becomes unstable. Such a relative orientation of the rigid tool against the rigid plane should be avoided, as it causes large uncertainty in the friction force.

B. Obstacle Mapping Accuracy

The obstacle mapping algorithm by exploratory collisions proposed in II-D is validated by showing the accuracy of obstacle mapping.

1) Method:

- The experimental setup is almost the same as in the previous experiment. However, in this experiment, the angle of the flat plate is fixed at 0 degrees. The small neodymum magnet as an obstacle on the plane is placed at one of the nine positions on the flat plate as shown in Fig. 5.
- As same as the previous experiment, the motion base is set so that the contact between the tool edge and the plate is maintained during the experiment. Therefore, it is ensured that the tool position is always inside the plane, that is, $\boldsymbol{p}_{\text{tool}} \in \boldsymbol{l} \subset \mathcal{P}$.
- The path of the motion base for each trial is also same as the previous experiment. However, the obstacle mapping algorithm shown in **Algorithm 1** is performed in parallel.
- Based on the proposed algorithm, the tool position is measured when the detected collision is judged to be sufficiently at the center. This value is memorized as the estimated position of the obstacle, i.e., $\hat{\boldsymbol{p}}_{\text{obs}} = \boldsymbol{p}_{\text{tool}}$.
- In the proposed algorithm, the setting of the contact location function $\gamma_{\Delta t}$ is crucial. In this experiment, the function is set as follows:

$$\gamma_{\Delta t} = \begin{cases} \text{'Left'} & w < -\delta \\ \text{'Right'} & w > \delta \\ \text{'Center'} & \text{Otherwise} \end{cases} \tag{3}$$

$$w := \int_{t^*-\Delta t}^{t^*} \boldsymbol{s}^T \begin{bmatrix} \boldsymbol{f}_{\text{s}}(\tau) \\ \boldsymbol{m}_{\text{s}}(\tau) \end{bmatrix} d\tau \tag{4}$$

where $\delta = 0.015$ Ns, $\Delta t = 0.7$ seconds, and $\boldsymbol{s} = [0\ 1\ 0\ 0\ 0\ 0]^T$. These values are set by trial and error.

- The nine positions for the magnet as an obstacle on the plane are measured in advance by a depth camera (Real Sense D415, Intel Co.) that is equipped with the motion

base. In each measurement, a marker for the depth camera is attached to the magnet for better accuracy. The measured positions for the magnet are used for the true position of the obstacle $\boldsymbol{p}_{\text{obs}}$.

2) Result: Fig. 6 shows the scatter diagram of the estimation error in obstacle position in the depth (x) direction and the lateral (y) direction. In this diagram, the horizontal and vertical axes show the percent error for a tool edge length of 0.68×10^{-1} meters. The error mean for nine measurements is plotted by '+'. The probability density assuming a normal distribution is depicted as a heat map. From this scatter diagram, we can see good accuracy and precision was achieved even though the manipulator is highly flexible, and the shape estimation algorithm is completely based on the rod model.

C. Quick Scooping

In this section, demonstration of quick scooping task is explained in order to show usefulness of Roddy. If the friction coefficient between an object to be scooped and the environmental flat plane is low, a sufficiently high speed of scooping motion is needed. Otherwise, the object may be pushed by the tool before scooping. However, if there is invisible obstacle on the plane in front of the manipulator, such a high speed motion is dangerous. Strong collision to the invisible obstacle may damage the manipulator. Based on this consideration, we take a two-step strategy where first the obstacle mapping algorithm will be conducted, and then a quick scooping motion with a high speed will be performed.

1) Method:

- The experimental setup is almost the same as in the previous experiment. In this experiment, two disk-shaped objects to be scooped are placed on the flat plate as shown in Fig. 7. Each object is 3D-printed disk made of ABS with 20 mm thick, 100 mm in diameter, and has a fillet with a radius of 10 mm on the edge. The positions of the objects are measured by the depth camera mounted on the motion base. The point cloud data obtained from the depth camera is classified and divided into point clouds for each object. The KD-Tree[11] is used as the classification algorithm.
- A small neodymum magnet is also placed on the flat plate in front of one of the two objects as an obstacle. Note that in this experiment a marker for the depth camera is not attached to this magnet. Therefore, this magnet is invisible from Roddy.
- The initial configuration of the motion base is same as the two previous experiments so that $\boldsymbol{p}_{\text{tool}} \in \boldsymbol{l} \subset \mathcal{P}$.
- Before a scooping task, the proposed obstacle mapping algorithm is performed. If an obstacle is mapped in front of an object, Roddy declines to scoop the object. Otherwise, the tool of Roddy is moved toward the object at the speed of 0.4 m/s.

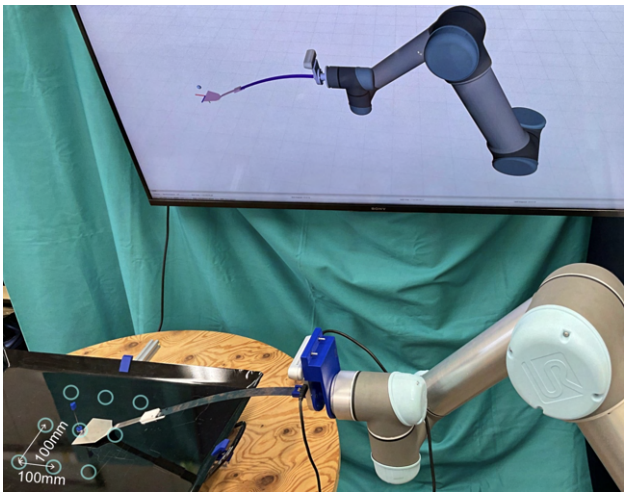

Fig. 5. Experimental setup for obstacle mapping accuracy

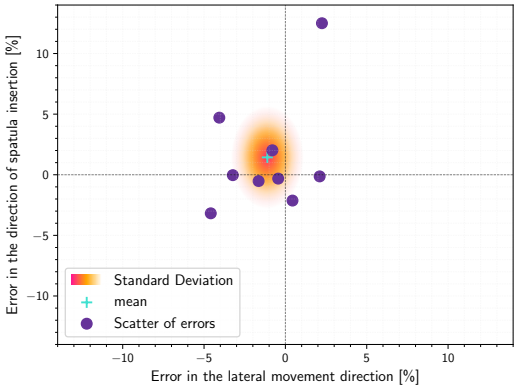

Fig. 6. Comparison of positions obtained by an RGB-D camera and those detected by the proposed method

2) Result: First, an obstacle magnet was placed on the flat plate in front of the gray object, which can be seen as a small white dot in the left photo of Fig. 7. The propose obstacle mapping algorithm successfully found the obstacle, then scooping of the gray object was judged to be dangerous. Next, an obstacle magnet was placed in front of the blue object as shown in the right photo of Fig. 7. In this case, any other obstacle was found in front of the gray object, then Roddy decided to scoop it. Due to a sufficient speed of the tool, the scooping task was successfully achieved as shown in Fig. 1.

This study focused on manipulation tasks in which a rigid spatula comes into contact with a rigid environment. In order to lift the object after scooping it up, some kind of mechanism is needed to change the stiffness of the rod. Since an elastic strip is used as the elastic rod, the stiffness differs depending on the direction. Therefore, when the side edge of the rod is facing upwards, deformation due to gravity is minimized. For example, by incorporating a rotating mechanism (rotational motor or locking mechanism) between the spatula and the rod, it is possible to achieve higher stiffness.

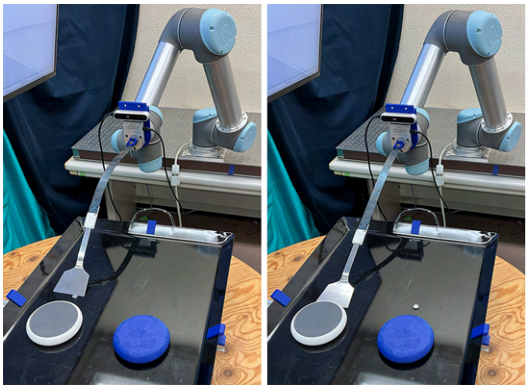

Fig. 7. Quick scoop action judgment (left): Roddy detected an obstacle (small white magnet) placed on a flat plate in front of the gray object using the object mapping algorithm. Therefore, no quick scooping action was performed on the gray object. (Right): Since there was no obstacle in front of the gray object, no collision occurred during the object mapping algorithm, and Roddy judged that it could be scooped up. A quick motion was then performed, and Roddy succeeded in scooping it up, which can be seen in Figure 1.

IV. REMARK

Fig. 8 shows two sets of four time graphs of measured forces, moment, and the integral of the force in the lateral (y) direction. The horizontal axis represents time. The first four graphs from the top (colored in blue) is the result when a collision occurred two times at the left side of the tool edge. On the other hand, the rest four graphs (colored in orange) is the result when a collision occurred two times at the right side of the tool edge. In both cases, the second collision occurred closer to the center of the tool edge than the first collision. For each set of graphs, the vertical axis means the force in the depth (x) direction (1st and 5th from the top), the force in the lateral (y) direction (2nd and 6th), the moment around the height (z) direction (3rd and 7th), and the time integral of the force in the lateral (y) direction (4th and 8th), respectively. The collisions on the right and left side occurred at approximately 1 and 6.25 seconds, and 1 and 6.32 seconds, respectively, which can be clearly observed from the sharp decrease from the force graphs in the depth (x) direction (1st and 5th). It can also be seen that the change in the graph due to the second collision is much smaller than the change in the graph due to the first collision in both cases. However, the force in the x-direction does not distinguish between the colliding sides. First, we thought that the moment around the z-direction can be used to judge the colliding sides because of a simple geometric consideration, but this value was found to be insensitive in comparison with noises, which can be observed from the 3rd and 7th graphs. Interestingly, the shape of the graph of y-force is very similar to that of x-force in the case of right side collision (1st and 2nd graphs) while those are symmetric in the case of left side collision (5th and 6th graphs), which means that the force in the y-direction can be used for judgement of the collision side. Because of the jagged shape of the y-force graphs at strong collision, the y-force integrals were employed instead (4th and 8th graphs), which justifies our selection of the contact location function

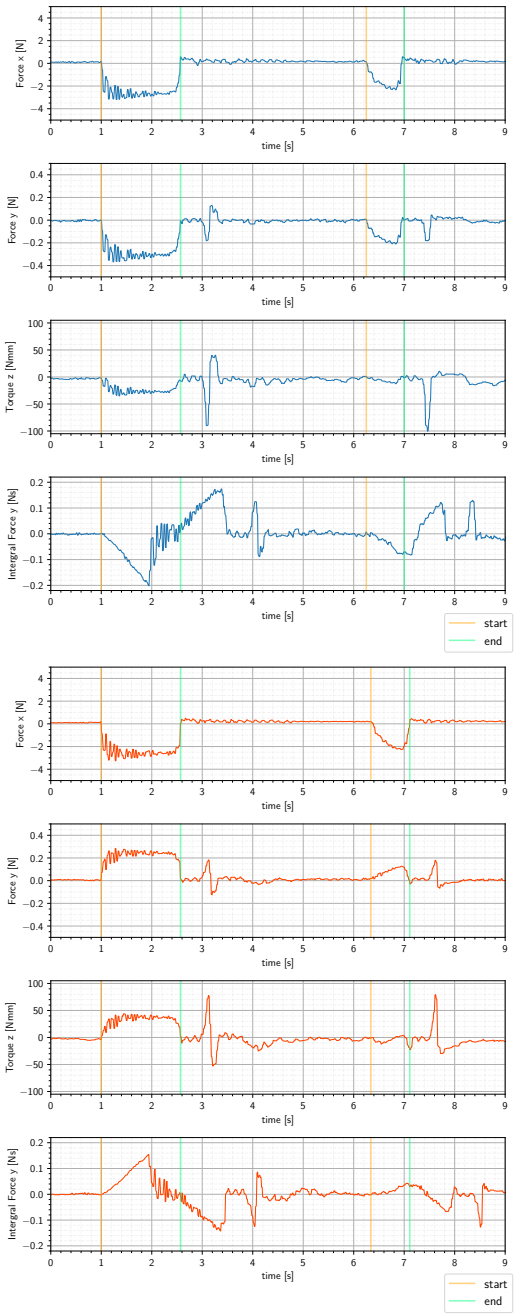

Fig. 8. Time Series Plot of Force Information (Blue: left side, Orange: right side)

expressed by equations (3) and (4).

V. CONCLUSION

This paper proposed Roddy, a manipulation system that incorporates rod elasticity in series between a conventional robot manipulator and a rigid tool. The high compliance of Roddy enabled successful calibration of the rigid tool to the environment rigid plane. An algorithm for obstacle mapping by exploratory collision was also developed. Here, the selection of a contact position function based on 6-axis force sensing was critical to improve the mapping accuracy. Finally, based on the obstacle mapping algorithm,

we demonstrated that quick scooping tasks can be safely accomplished by Roddy even in the presence of invisible obstacles on the plane.

The current prototype of the proposed robot system is rudimentary, and it is necessary to verify it from all angles while comparing it with other related methods. The execution time for scooping is still long and needs to be sped up. The depth mapping accuracy of the obstacles is not that bad, but it needs to be studied in more depth for improvement. The effect of design parameters on obstacle mapping needs to be clarified so that our robot system can operate in various environments. In addition, the effect of the material properties of the elastic rod needs to be investigated to improve the calibration accuracy. It would be desirable to extend the obstacle mapping algorithm so that it can identify the shape of obstacles. In addition, this algorithm needs to be tested on uneven rigid surfaces. Furthermore, future challenges include using Roddy to attempt more advanced tasks, such as unlocking and locking doors with keys and handling real food with viscosity.

REFERENCES

[1] N. Hogan. Impedance control: An approach to manipulation. PartsI-III. Trans. ASME J. Dyn. Systems Meas. Control, 107:1–24, 1985.

[2] P. -C. Yang, K. Sasaki, K. Suzuki, K. Kase, S. Sugano and T. Ogata, "Repeatable Folding Task by Humanoid Robot Worker Using Deep Learning," in IEEE Robotics and Automation Letters, vol. 2, no. 2, pp. 397-403, April 2017

[3] A. Sasagawa, K. Fujimoto, S. Sakaino and T. Tsuji, "Imitation Learning Based on Bilateral Control for Human–Robot Cooperation," in IEEE Robotics and Automation Letters, vol. 5, no. 4, pp. 6169-6176, Oct. 2020

[4] Y. Wang, C. Beltran-Hernandez, W. Wan , K. Harada, "An Adaptive Imitation Learning Framework for Robotic Complex Contact-Rich Insertion Tasks," in Frontiers in Robotics and AI, vol. 8, January 2022

[5] G. A. Pratt and M. M. Williamson, "Series elastic actuators," Proceedings 1995 IEEE/RSJ International Conference on Intelligent Robots and Systems. Human Robot Interaction and Cooperative Robots, Pittsburgh, PA, USA, 1995, pp. 399-406 vol.1

[6] S. Haddadin, A. De Luca and A. Albu-Schäffer, "Robot Collisions: A Survey on Detection, Isolation, and Identification," in IEEE Transactions on Robotics, vol. 33, no. 6, pp. 1292-1312, Dec. 2017

[7] H. Mochiyama, "Model validation of discretized spatial closed elastica," 2016 IEEE/RSJ International Conference on Intelligent Robots and Systems (IROS), Daejeon, Korea (South), 2016, pp. 5216-5223

[8] R. Takano, H. Mochiyama and N. Takesue, "Real-time shape estimation of Kirchhoff elastic rod based on 6-axis force sensor," 2017 IEEE International Conference on Robotics and Automation (ICRA), Singapore, 2017, pp. 2508-2515

[9] N. Nakagawa and H. Mochiyama, "Real-Time Shape Estimation of an Elastic Rod Using a Robot Manipulator Equipped with a Sense of Force," 2018 IEEE/RSJ International Conference on Intelligent Robots and Systems (IROS), Madrid, Spain, 2018, pp. 8067-8073

[10] Martin A. Fischler and Robert C. Bolles, Random sample consensus: a paradigm for model fitting with applications to image analysis and automated cartography, Communications of the ACM, Volume 24, Issue 6, 1981, pp. 381–395.

[11] Jerome H. Friedman, Jon Louis Bentley, and Raphael Ari Finkel. 1977. An Algorithm for Finding Best Matches in Logarithmic Expected Time. ACM Trans. Math. Softw. 3, 3 (Sept. 1977), 209–226.